VOL. 16, NO. 19, OCTOBER 2021 ISSN 1819-6608
ARPN Journal of Engineering and Applied Sciences

www.arpnjournals.com

ASSESSMENT OF VISCOUS MODELS ON THE SIMULATION OF LOW CUT-OFF WIND TURBINE BLADE

Zahir U. Ahmed, Mohammad Mashud and Shabnoor M. Joty
Department of Mechanical Engineering, Khulna University of Engineering and Technology, Khulna, Bangladesh
E-Mail: mdmashud@me.kuet.ac.bd

ABSTRACT

Renewable energy has received large attention in both developed and developing countries in the world as an alternative to the fossil fuel based energy. Wind energy is becoming one of the popular means to harness energy from renewable sources. Although abundant research had previously been undertaken for high Reynolds number, research on different viscous models at low Reynolds number is limited in the world. As such, in this paper a numerical study is performed for low speed wind turbine blades where five viscous models such as laminar, RNG k-ε model, SST k-ω, Transitional SST, and Transitional k-kl-ω, and four airfoils, namely NACA-4412, NACA-4421, NACA-4418 and NACA-2412 are chosen for comparative study. Numerical simulation was done via finite volume based software. The result shows that laminar, RNG k-ε and SST k-ω models are able to predict general behavior of both profiles, whereby laminar and SST k-ω models are able to capture stall angle. Whilst all the viscous models predicts well the pressure coefficient on lower surface of the airfoil, but only laminar and RNG k-ε models perform better in the upper surface of airfoil. The drag is found to be higher with the increase of angle of attack (AOA). The lift to drag ratio increases with increase of AOA but decrease after a certain point.

Keywords: aerodynamic, wind turbine, cfd, viscous model, lift coefficient and pressure.

1. INTRODUCTION

Wind energy is a ubiquitous form of renewable energy sources, and has been widely used in many applied fields, such as generating electricity, propel sailboats and water pumps. Power is typically generated from large-scale wind turbines in every part of the world, where wind speeds are generally large. Horizontal axis wind turbines (HAWT) are becoming more popular day by day but to improve the aerodynamic performance of degrading blades, passive flow control devices, such as vortex generators are gaining importance. With the increasing demand of energy over the world, harvesting energy from wind sources can be an alternative energy solution. Designing low cut-off wind turbine blades is still a challenge for its effective use.

Abundant researches are available in the literature on the fundamental behavior of wind turbine blades and methods for their performance improvements. Both horizontal axis and vertical axis wind turbines are typically considered for power generation in different situations. Siavash *et al*. [1] showed a new mathematical modeling of shrouded wind turbine, which introduces new equations to predict the power coefficient and speed up ration effects. Mereu *et al.* [2] showed scale-resolving methods superior in stall angle simulation compared to Reynolds-Averaged Navier-Stokes (RANS) models. Blade shape was found to have significant effect on the performance of a wind turbine. Large scale wind turbines are used widely today but small scale wind energy harvesting is also an emerging field.

Vertical axis wind turbine (VAWT) is also getting more popular now-a-days. So many numerical and experimental works has been done on VAWT. Lositano *et al*. [3] studied the performance of a 5 kW three-bladed H-rotor Darrieus VAWT with cambered tubercle leading edge (TLE) blades. Meana-Fernández *et al*. [4] introduce the Richardson extrapolation method for the Computational Fluid Dynamics (CFD) simulation of VAWT and analyze the flow field. Chai *et al*. [5] alanyzed the performance of H-type Darrieus VAWT rotor with and without the winglets and the study showed that winglets increase the overall torque-generating, but does not improve it at every azimuthal angle for each blade. The angle of attack (AOA) is a dominant parameter for generating aerodynamic force for a wind turbine. Elsakka *et al*. [6] completed a CFD analysis of the effect of AOA for a VAWT blade. The results illustrates the advantages of sinusoidal variable pitch configuration could enhance the overall performance of the. Concurrently, Zhang *et al.* [7] presented the effect of winglets for VAWT and showed that winglets assist to maintain the pressure difference between the two sides of the blade. This weakens the tip vortex and improves the aerodynamic efficiency of the surface near the blade tip. Wang *et al*. [8] conducted a study on aerodynamic performance of deformable blade for VAWT. The study shows that, within an appropriate range of deformation factor, the blade aerodynamic performance can be improved by deforming.

Horcas *et al.* [9] showed an interesting approach of introducing flaps for wind turbine blades aiming to analyze the impact of trailing edge flaps activation on Vortex Induced Vibrations (VIV) suppression. Another interesting approach of generating wind energy from coaxial rotor wind turbine was done by Mashud *et al*. [10]. They showed that the assembly has a better dynamic balance with reduced noise. A CFD based support vector regression to determine the optimum smooth twist for wind turbine blades is performed by Kaya [11]. Ni *et al*. [12] investigated slotted blade in order to improve performances by deploying a novel slot design. Building-mounted wind turbines are new concept and may become popular in urban areas. However, limited research is available on this. Arteaga-Lopez et al. [13] performed a CFD analysis on

advanced methodology for feasibility studies on building-mounted wind turbines installation in urban environment. A similar work has been conducted by Rodrigues and Lengsfeld [14] to develop a computational system to improve the layout of a wind farm considering wake effect.

Experimental study of the wind turbine blade is a very important approach to find suitable blades for practical use. Costantini [15] also perform an experimental study for the mid-span sections of the modern rotor blades. Another experimental study on dynamic aerodynamic characteristics of a yaw-oscillating wind turbine airfoil is done by Li *et al.* [16]. Their observations showed that the aerodynamic curves of the yaw-oscillating airfoil have an obvious hysteresis effect and the hysteresis loop of different aerodynamic parameter show different shapes. Li *et al.* [17] studied HAWT blade using Laser Doppler Velocimetry (LDV) measurement. Wind turbine noise has become an issue for the design engineers now. Reasons behind noise generation and its mitigation is also an important topic now. Deshmukh *et al*. [18] provided a detailed study on various research works on reducing wind turbine noise. Small scale wind turbine designing is a promising field of wind energy harvesting. Lin *et al.* [19] introduce a new design of complex airfoil small wind turbine, which is suitable for public utility applications and has a better efficiency than previous designs. Another experimental and computational work on small wind turbine is conducted by Lipian *et al.* [20]. They have shown a fast track integrated system of computational and experimental work to design a small wind turbine within a very short time.

Designing wind turbine blades for low speed regions is a fascinating field of interest for the researchers for decades. In 1998, Giguere and Selig [21] proposed a new airfoil for small horizontal axis wind turbines for a lower range of Reynolds numbers. Singh and Ahmed [22] have worked on blade design and performance testing of wind turbine rotor for low wind speed. They proposed a new 2-bladed rotor design using the airfoil AF300 and a pitch angle 18˚, which performs better than traditional 3-bladed rotors. Another study on large HAWT for low wind speed regions was conducted by Li *et al. [*23]. The starting behavior analysis is the primary concern of designers, but is also important to maximize the power output. Wright and Wood [24] conducted a field testing on a 3-bladed 600W HAWT and found that, most starting torque generates from near the hub area and most power extracting torque generates in the tip area. A similar work is done by Ebert *et al.* [25]. Different S-series wind turbine blade profiles developed by National Renewable Energy Laboratory (NREL) have analyzed at a low speed using finite volume method (FVM) by Sayed *et al*. [26].

Low speed airfoils are the most vital element for designing a blade of wind turbines to harvest power at a low Reynolds number. Plenty of research has been done on investigation of the aerodynamic behavior of low speed airfoils. Shen *et al.* [27] investigated the curvature effects on aerodynamic behavior of Eppler 387, a low Reynolds number airfoil used for small wind turbines. It is shown that a better curvature distribution leads to higher energy output efficiency. Xi et al. [28] showed that gurney flaps enhance the pre-stall lift for low Reynolds number and also found that gurney flaps can delay the transition onset position at small angle of attack (α). Flow separation and transition of airfoil is studied by Dong *et al.* [29]. The study found significant change of flow structure for a Reynolds number ranges between 300000 to 500000. Another study conducted by Deng et al. [30] showed that at a very low Reynolds number (within 100 to 1300), the flow become very sensitive as well as the angle of attack (α) and the wake dynamics is complex. They have found different branches on the Strouhal-Reynolds number relationship curves. Ilio *et al*. [31] studied NACA 0012 airfoil at low Reynolds number with hybrid lattice Boltzmann method (HLBM) and showed the capability of this method near solid curved walls. Xfoil is a very renowned and powerful tool for designing subcritical airfoils particularly applicable to low Reynolds number airfoils. The methods and algorithms Xfoil uses for low speed airfoil analysis is presented in a research paper by the inventor of Xfoil, Drela [32]. Morgado *et al.* [33] conducted a comparison study of Xfoil against CFD data for high lift low Reynolds number airfoils. Another similar works of numerical and statistical analysis of aerodynamic characteristics of low speed airfoil using Xfoil and JMP (a statistical analysis tool) is investigated by Chua *et al.* [34]. On wind turbine dedicated. Timmer and Rooij [35] used a modified version of Xfoil named RFoil on airfoils developed by Delft University of Technology (DUT) for the effect of Gurney flaps, trailing edge wedges, vortex generators and trip wires. Zhang *et al.* [36] showed an approach of design optimization using characteristic parameters control. Their algorithm use Xfoil tool for predicting flow behavior.

Numerical analysis and simulation of an airfoil is a hideous job. To simulate low Reynolds number airfoils, proper viscous model has to be chosen for better output. Wauters and Degroote [37] conducted a comparative study on four different variations of a low Reynolds number model operating at high angles of attack (α). Four different variations considered are: Menter's k-ω SST model with Wilcox's low-*Re* modification, Menter & Langtry's $(k-\omega\ SST)\ \gamma - Re_\theta$ model, it's simplified $(k-\omega\ SST)\ \gamma$ model and Walters & Cokljat's $k-kl-\omega$ model. The authored performed detailed comparison of models, but with no verdict about the best performing model. Lee et al. [38] conducted a similar comparative study with the models: three-dimensional large-eddy simulations (3-D LES), two-dimensional laminar simulations (2-D Lam), Reynolds-averaged Navier–Stokes simulations with Baldwin–Lomax (2-D RANS (BL)) and Spalart–Allmaras (2-D RANS (SA)) models. They suggested that 2D-LAM method without any turbulence models can be used for qualitative study of airfoil aerodynamic characteristics at low Reynolds number. Aftab et al. [39] conducted another comparative study of turbulence models to analyze separation bubbles formation on an airfoil's surface at low Reynolds number. The models they used are one equation Spallart Allmars (S-A), two equation k-ω SST, three equation Intermittency (γ) SST, k-kl-ω and finally, the four equation transition γ-Re_θ SST. The paper illustrates, S-A is a very widely used model and can provide a better result for

initial guess and k-ω SST is a suitable model for external turbulent flows and intermittency SST also produce almost similar results like k-ω SST. The k-kl-ω gave a good result only for lower angle of attack (6˚) but consume more computational time than any other models. For their particular study only γ-Re_θ SST model can generate reliable results compared to other models not only for lower α but also for higher α at a moderate computational time. Santo *et al.* [40] predicted by a numerical analysis that the performance and the loads are highly affected by the atmospheric boundary layer. In this regard, they used unsteady RANS approach and k-ε turbulence model. Kim and Suh [41] performed an experimental and numerical investigation on power characteristics on a 300W horizontal axis wind turbine with wave winding type axial flux permanent magnet (AFPM) generator and it eventually increase the efficiency of the HAWT and also minimize the cost. Mohamed et al. [42] carried out a numerical analysis on three-bladed Darrieus vertical axis wind turbine performances (torque and power outputs) using 25 different sectional profile airfoils from different families. They used unsteady (transient) Reynolds-Averaged-Navier-Stokes (URANS) calculation and the optimization showed that the modified design has 16% improved power coefficient. Singh et al. [43] performed an experimental and numerical analysis on several low speed airfoils at different Reynolds numbers for small HAWT. They use CFD along with Particle Image Velocimetry (PIV) and smoke flow visualization apparatus and it illustrates that, for the airfoil AF300, the flow attached with the surface for *Re* as low as 75,000 at an angle of 14˚. Thomareis and Papadakis [44] performed a numerical study on the effect of trailing edge shape on the separated flow characteristics of an airfoil at low Reynolds number.

Though plenty of numerical and experimental works on low Reynolds number is done already, a very few works have completely focused on comparing numerical methods or viscous models. Designing low cut-off speed wind turbine blade involves with numerical study of airfoils at low wind speed. So choosing a better viscous model is the key of getting reliable simulation result for the design and optimization of suitable airfoils for wind turbine blades. In this paper, the focus is confined within exploring the results of different viscous models and comparing the results with experimental ones to validate and identify the best models for predicting flow behavior of low speed airfoils at low Reynolds number.

2. COMPUTATIONAL SET–UP

The governing equations for the current problem are continuity equation and momentum equations. Momentum equations include both laminar and turbulent conditions, whereby turbulent flow governing equations are considered as RANS equations. For the numerical simulation, a commercial software package ANSYS Fluent v16 was used to solve the governing equations. The methodology consists of profile selection for low wind speeds, mesh generations, boundary conditions and viscous models choosing. A typical airfoil profile with their details is shown in Figure-1.

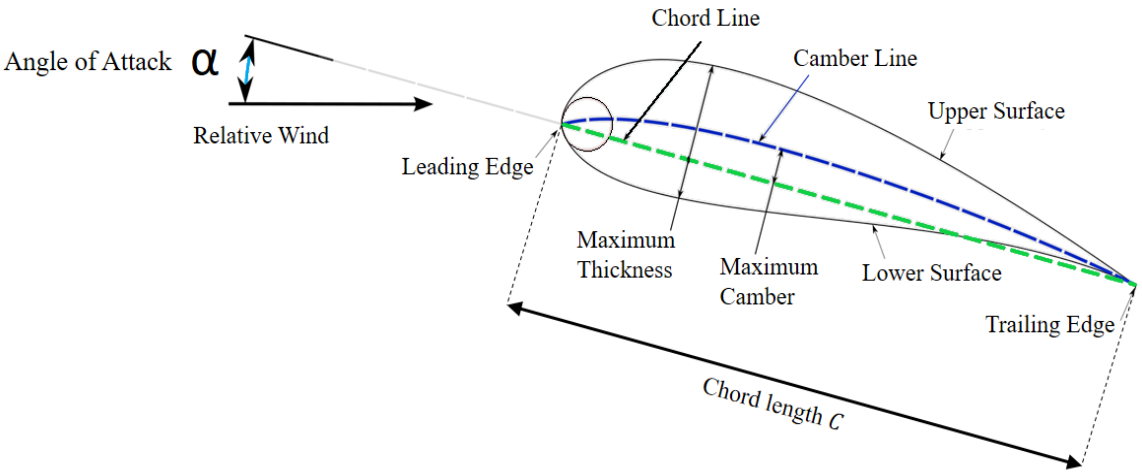

Figure-1. The schematic of an airfoil with relative air flow.

2.1 Profile Selection

There are number of airfoils, which are believed to be effective and suitable for low wind speed cases, available in the literature. Examples of these airfoils are NACA 4412, NACA 4418, NACA 4421, NACA 63412 and NACA 63415. Among these variations, only NACA 4412, NACA 4421, NACA 4418, and NACA 2412 are considered in this study due to their availability of detailed experimental data. The geometry of the selected profiles is shown in Figure-2.

2.2 Mesh Generation

The numerical domain is a C-mesh, consists of a flow field, inlet, outlet and the airfoil body. Structured mesh is used for faster iteration. Quadrilateral mesh element is chosen here. The density of mesh is higher near the surface of the airfoil to capture near-surface flow physics. Figure-3 presents mesh independency test with six different mesh elements, namely 7k, 16k, 33k, 59k, 103k and 290k. It appears that change in C_L is found to be the minimal. Table1 shows the relative errors among the meshes, and a mesh of

around 103k elements is used finally for all models. The detailed mesh around the airfoil and near the surface is depicted in Figure-4. A second-order upwind discretization technique and pressure based coupled solver is used. Atmospheric air is used as fluid medium, with density (ρ) 1.225 kg/m^3 and viscosity (μ) 1.789x10-5 kg/ms. Velocity inlet is chosen in the domain inlet with uniform wind velocity of 3 m/s. The corresponding Reynolds number (Re) and Mach number is 20,000 and 0.0087, respectively. Atmospheric pressure is considered at the pressure outlets. No slip boundary condition is applied at the airfoil surface. The convergence is assumed to achieve when the residuals of the variables reaches to 10^{-5}. The boundary conditions are shown in Figure-5.

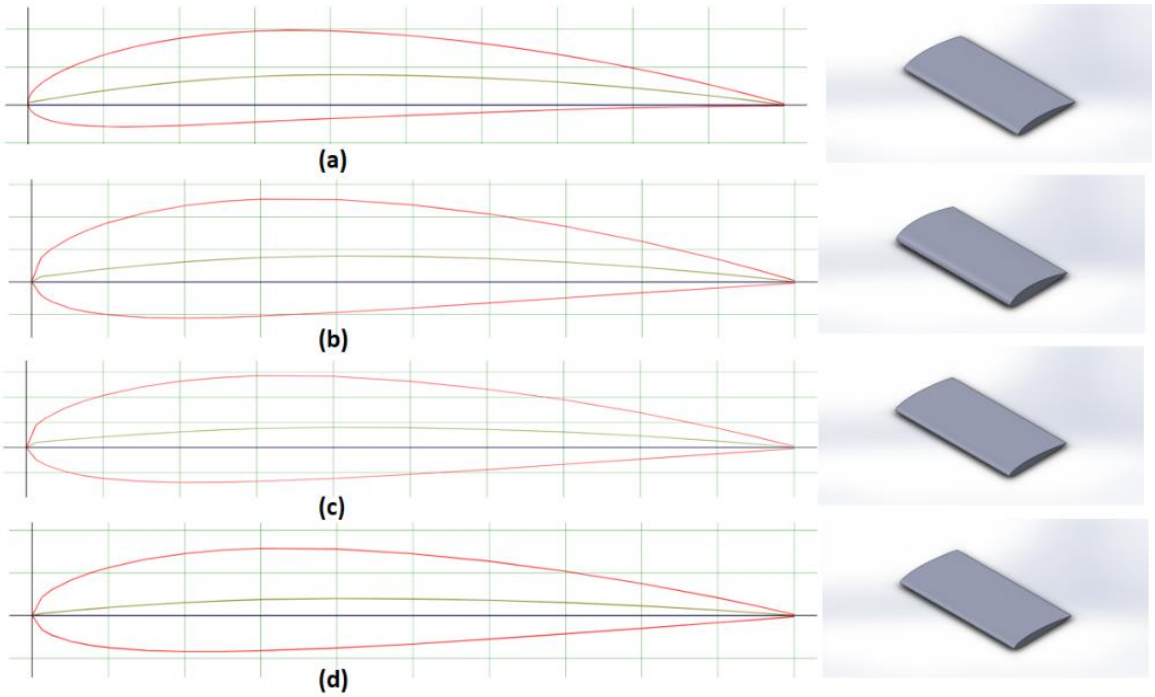

Figure-2. The profile of airfoils used for this study and their SolidWorks models: (a) NACA 4412 (b) NACA 4421, (c) NACA 4418, and (d) NACA 2412.

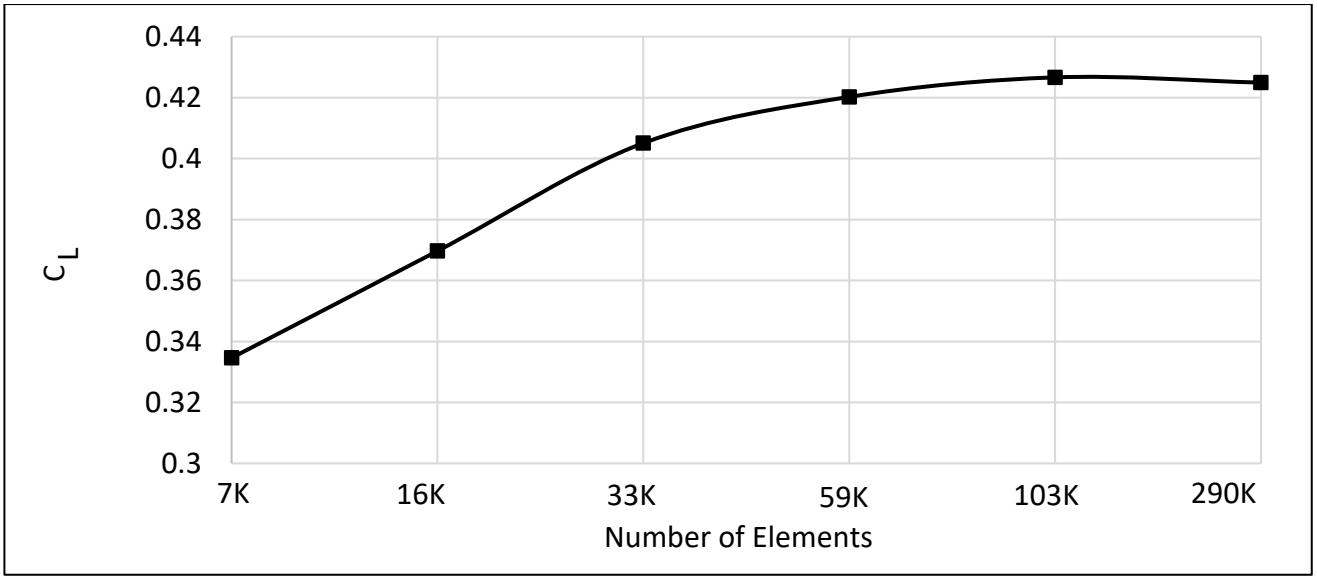

Figure-3. Mesh independency study for different number of meshes.

Table-1. Details of mesh independency test.

S. No	Number of Elements in Mesh	Lift Coefficient (C_L)	Deviation between two consecutive mesh	Deviation from the last mesh (%)
1	7836	0.3346	9.4875	21.25
2	16134	0.3696	8.7360	12.99
3	33678	0.4050	3.6078	4.67
4	59052	0.4202	1.5017	1.10
5	103694	0.4266	0.4049	0.40
6	290260	0.4249	-	0

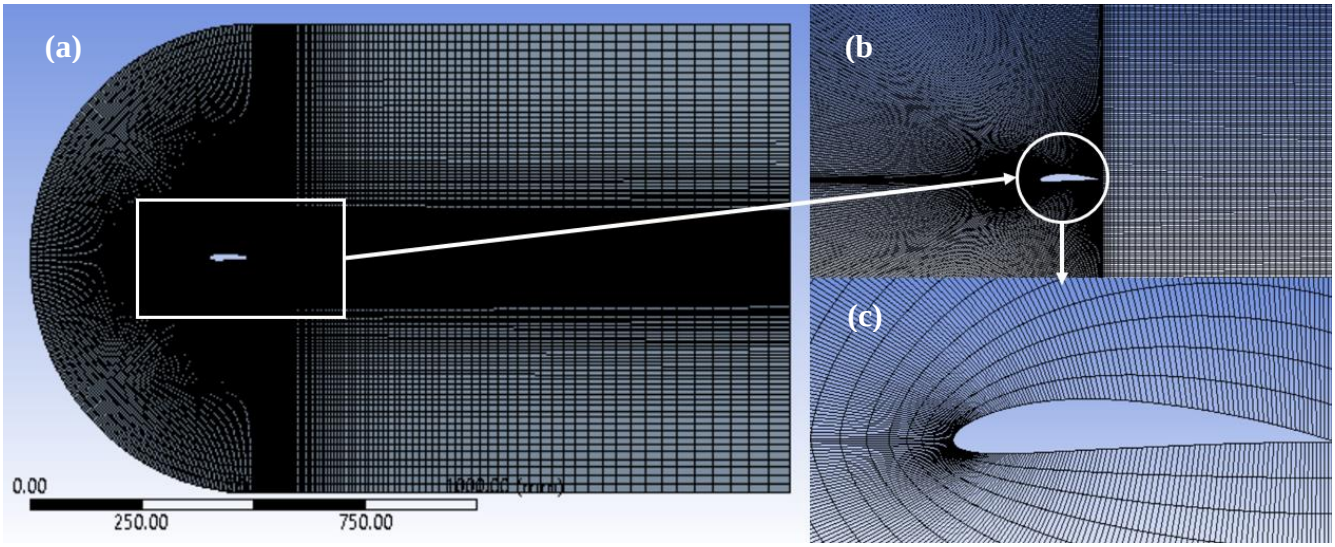

Figure-4. Computational grid of structured mesh for (a) the entire domain (b) magnified view (c) mesh around the baseline airfoil.

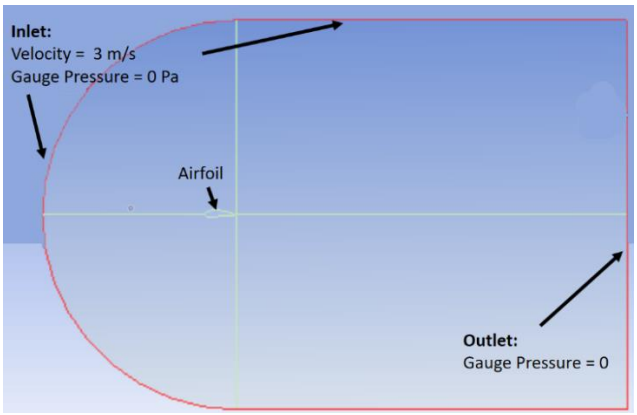

Figure-5. Computational domain with boundary conditions.

2.3 Viscous Models

Different viscous models are available in standard ANSYS Fluent suit for numerical simulations. However, following models are used in this study, and they are chosen based on their superiority in wall bounded flows.

The models are:

a) Laminar
b) Transition SST model
c) K-ω SST model
d) RNG k-ε model
e) Transition k-kl-ω model

The Navier-Stokes Equations used by the solver in vector form is as follows [45]:
Continuity equation,

$$\nabla \cdot \vec{V} = 0 \quad (1)$$

Momentum equation,

$$\rho \frac{D\vec{V}}{Dt} = -\nabla p + \rho \vec{g} + \mu \nabla^2 \vec{V} \quad (2)$$

2.3.1 Laminar

Laminar model is the model where the flow is considered as a laminar flow.

2.3.2 Transition SST model

The transport equation for Transition SST model for the intermittency γ is defined as [45]:

$$\frac{\partial(\rho\gamma)}{\partial t}+\frac{\partial(\rho U_j\gamma)}{\partial x_j}=P_{\gamma 1}-E_{\gamma 1}+P_{\gamma 2}+E_{\gamma 2}+\frac{\partial}{\partial x_j}[(\mu+\frac{\mu_t}{\sigma_\gamma})\frac{\partial\gamma}{\partial x_j}] \quad (3)$$

The transition sources are defined as:

$$P_{\gamma 1}=2F_{length}\rho S(\gamma F_{onset})^{c_{\gamma 3}} \quad (4)$$

$$E_{\gamma 1}=P_{\gamma 1}\gamma \quad (5)$$

Where S is the strain rate magnitude. F_{length} is an empirical correlation that control the length of the transition region. The destruction sources are defined as follows:

$$P_{\gamma 2}=(2c_{\gamma 1})\rho\Omega\gamma F_{turb} \quad (6)$$

$$E_{\gamma 2}=c_{\gamma 2}P_{\gamma 2}\gamma \quad (7)$$

Here Ω is the vorticity magnitude.

2.3.3 K-ω SST model

The transport equation is similar to standard $k-\omega$ model [45]:

$$\frac{\partial}{\partial t}(\rho k)+\frac{\partial}{\partial x_i}(\rho k u_i)=\frac{\partial}{\partial x_j}(\Gamma_k\frac{\partial k}{\partial x_j})+\tilde{G}_k-Y_k+S_k \quad (8)$$

and

$$\frac{\partial}{\partial t}(\rho\omega)+\frac{\partial}{\partial x_i}(\rho\omega u_i)=\frac{\partial}{\partial x_j}(\Gamma_\omega\frac{\partial\omega}{\partial x_j})+\tilde{G}_\omega-Y_\omega+S_\omega \quad (9)$$

Here $\tilde{G}_k$ is the generation of turbulence kinetic energy due to mean velocity gradient. $\tilde{G}_\omega$ represents the generation of ω. Γ_k and Γ_ω represent the effective diffusivity of k and ω, respectively. Y_k and Y_ω represent the dissipation of k and ω due to turbulence. D_ω is the cross-diffusion term. S_k and S_ω are user-defined terms.

2.3.4 RNG k-ε model

The transport equation for the RNG k-ε model is defined as [45]:

$$\frac{\partial}{\partial t}(\rho k)+\frac{\partial}{\partial x_i}(\rho k u_i)=\frac{\partial}{\partial x_j}(\alpha_k\mu_{eff}\frac{\partial k}{\partial x_j})+G_k-G_b-\rho\varepsilon-Y_M+S_k \quad (10)$$

and

$$\frac{\partial}{\partial t}(\rho\varepsilon)+\frac{\partial}{\partial x_i}(\rho\varepsilon u_i)=\frac{\partial}{\partial x_j}(\alpha_\varepsilon\mu_{eff}\frac{\partial\varepsilon}{\partial x_j})+C_{1\varepsilon}\frac{\varepsilon}{k}(G_k+C_{3\varepsilon}G_b)-C_{2\varepsilon}\rho\frac{\varepsilon^2}{k}-R_\varepsilon+S_\varepsilon \quad (11)$$

Here G_k is the generation of turbulence kinetic energy due to the mean velocity gradients. G_b is the generation of turbulence kinetic energy due to buoyancy. Y_M represents the contribution of the fluctuating dilatation in compressible turbulence to the overall dissipation rate. The quantities α_k and α_ε are the inverse effective Prandtl numbers for k and ε respectively. S_k and S_ε are user-defined source terms.

2.3.5 Transition k-kl-ω model

The transport equation for Transition k-kl-ω is defined as [45]:

$$\frac{Dk_T}{Dt}=P_{K_T}+R+R_{NAT}-\omega k_T-D_T+\frac{\partial}{\partial x_j}[(\upsilon+\frac{\alpha_T}{\alpha_k})\frac{\partial k_T}{\partial x_j}] \quad (12)$$

$$\frac{Dk_L}{Dt}=P_{K_L}+R+R_{NAT}-D_L+\frac{\partial}{\partial x_j}[\upsilon\frac{\partial k_L}{\partial x_j}] \quad (13)$$

$$\frac{D_\omega}{D_t}=C_{\omega 1}\frac{\omega}{k_T}P_{K_T}+(\frac{C_{\omega R}}{f_W}-1)\frac{\omega}{k_T}(R+R_{NAT})-C_{\omega 2}\omega^2+C_{\omega 3}f_\omega\alpha_T f_W{}^2\frac{\sqrt{k_T}}{d^3}+\frac{\partial}{\partial x_j}[(\upsilon+\frac{\alpha_T}{\alpha_\omega})\frac{\partial\omega}{\partial x_j}] \quad (14)$$

3. RESULT AND DISCUSSIONS

In this section, assessment of laminar and various turbulence models are presented first, with numerical results validation against benchmark experimental data. In this regard, various aerodynamic parameters, such as lift coefficient, drag coefficient, coefficient of pressure, lift-to-drag ratio, and streamlines are discussed for different controlling parameters.

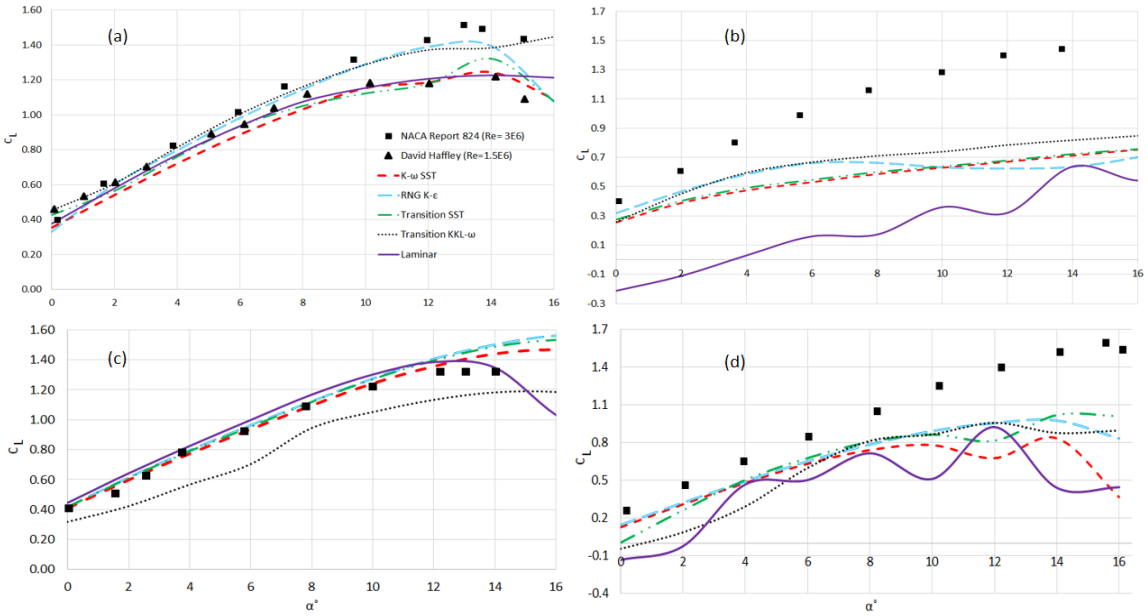

Figure-6. A comparison between the numerical and the experimental data [46-47] according to the coefficient of lift (C_L) vs angle of attack (α) for the viscous models and and airfoils: (a) NACA 4412, (b) NACA 4418, (c) NACA 4421, and (d) NACA 2412.

Figure-6 shows the coefficient of lift against angle of attack (α) in the range 0˚-16˚ at a low wind speed for NACA profiles (a) 4412, (b) 4418, (c) 4421, and (d) 2412. Five different viscous models with two experiemental data [46-47]. Figure-6 (a) illustrates that, for NACA 4412 laminar voscous model performs better than any other models at low Reynolds number (Re = 1.5×10^6). Laminar model can predict the result upto stall angle and after the stall laminar model can no longer predict accurate results. It is found difficult to predict the sharp downward tendency of C_L by using laminar model and the reason is after stall angle turbulance behavior dominate the flow. On the other hand, more complex models like RNG k-ε model outperforms other models at a little higher Reynolds number (Re = 3.0×10^6), even after stall. The model SST k-ω and Transitional SST also performs very well at low Reynolds number (Re = 1.5×10^6) even after stall. The model Transition k-kl-ω produce anomalous data and can not predict accurate results. For NACA 4418 (Figure-6 (b)), the accuracy of all the models are poor, with deviation after 6˚. Transitional k-kl-ω, Transitional SST, and SST k-ω follows the characteristic of the experimental data but not accurate in terms of magnitude. In contrast, laminar and RNG k-ε model produce inacurate results and perform poorly. Figure-6 (c) shows that, all viscous models predict general flow behavior well except Transition k-kl-ω. In this regard, laminar model captures experimental datta outstandingly and even produce better results for flow after stall angle. In Figure-6(d), almost all models performed poorly, but with worst behavior for laminar model. Only RNG k-ε performed comparatively better than other models. All these models daviate from the experimental results from α=10˚. Finally, it appears that Transitional SST, RNG k-ε and SST k-ω shows better performance considering all airfoils for low wind velocities.

Figure-7 presents drag coefficient (C_D) for the effect of angle of attack in the range α= 0˚-16˚ to compare different models considered in this study. Figure-7 (a) shows that all the models predict similar results except a sudden jump from α=12˚ for RNG k-ε and a weak dip from α= 14˚ from Transition SST. Overall, C_D is found to be independent of viscous models up to the stall. In Figure-7 (b), Transition SST and SST k-ω predict exactly similar results, with RNG k-ε shows similar behavior. Transition k-kl-ω is found to be the worst deviating from α=4˚. In Figure-7 (c) all the viscous models show very similar results, with Laminar and Transition k-kl-ω prodcue a slightly different results after α=13˚. In Figure-7 (d) all models produce different results after α=5˚. Similarly to, 5(b) and 5(c), Laminar and Transition k-kl-ω displays consitently different results than other modesl indicating not performing well to predict drag coefficient. All these curves of Figure-7 shows that, drag force increses proportionally with the angle of attack (α). However, with the increase of α, tubulance dominate the flow behavior and so it becomes more difficult to predict flow behavior accurately. In general, higher drag force can be obtained by increasing α, and there must have an optimum if one compares with lift increasement with α, which will, however be discussed later in this study.

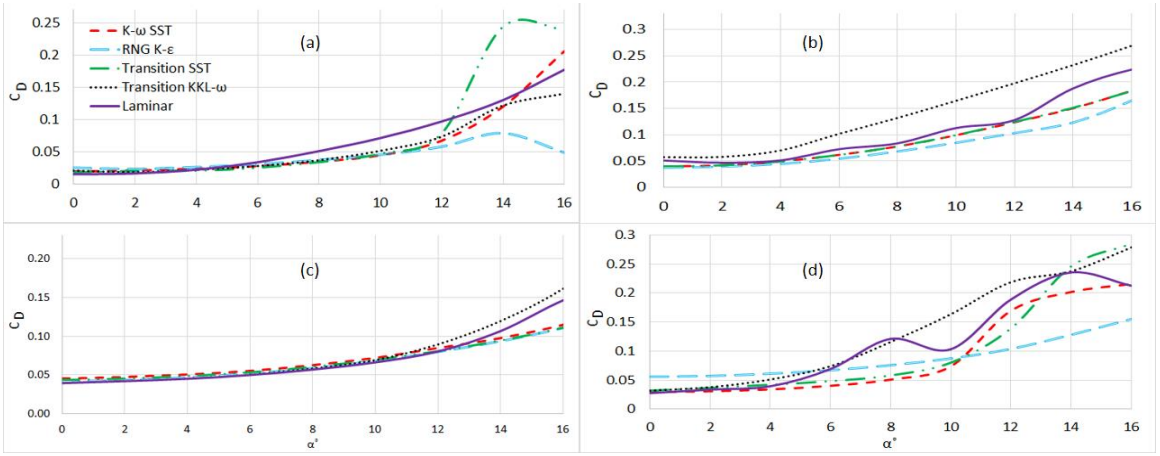

Figure-7. A comparison of numerical data between the viscous models for the coefficient of drag (C_D) vs angle of attack (α) for the airfoils: (a) NACA 4412, (b) NACA 4418, (c) NACA 4421, (d) NACA 2412.

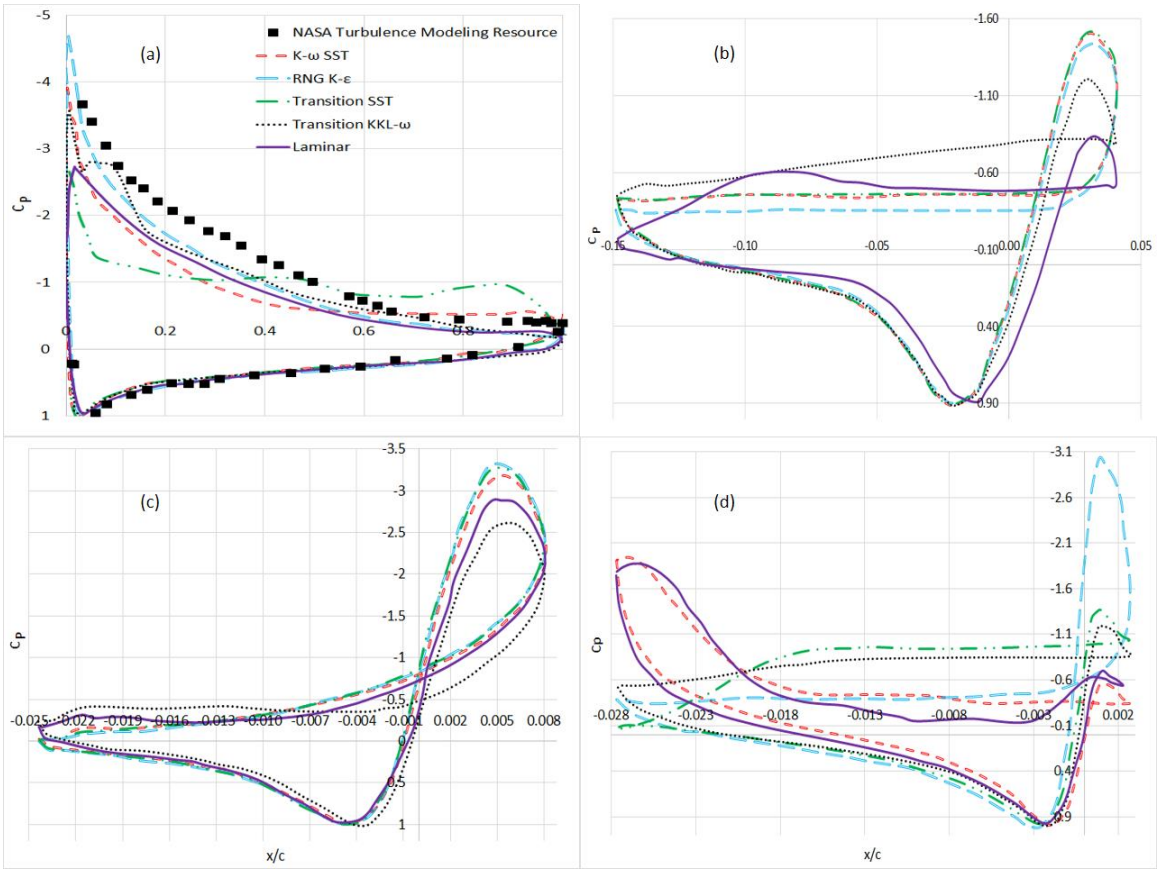

Figure-8. A comparison of numerical and experimental data [48] between the viscous models for the coefficient of pressure (C_P) vs angle of attack (α) for the airfoils: (a) NACA 4412, (b) NACA 4418, (c) NACA 4421 and (d) NACA 2412

Figure-8 depicts distribution of pressure coefficient (C_P) of different airfoil profies along their surface for various viscous models at or around stall angle i.e. at α=14˚. Figure-8 (a) also shows a comparison of the numerically computed coefficient of static pressure with experiemtnal data [48] at a low Reynold number (Re = 1.52×10^6). In these figures, the pressures of upper surface shows in the upper side (negative magnitude side of the plot) and bottom surface is in the down side for convenience. The figure shows that, for the lower surface of the airfoil NACA 4412, all the models performed very well and predict the experimental data almost accurately. This can be attributed to the no flow separation along the lower surface. In contrast, a significant and strong

deviations are observed among the models as compared to experimental data in the upper side of the airfoil. Though no model can capture the physics properly, RNG k-ε, k-ω SST and Laminar model able to resolve the characteristics, but with reduced magnitude of C_P. The discrepancy between experimental and numerical result may be ascribed to the large variations of Reynold number. In the simulation Reynolds number equals to 20,000 and in the experiment [48] it is $Re=1.52\times10^6$. Additionally, for the upper surface of the airfoil at higher α flow will be dominated by turbulance and after stall angle it is very difficult to predict the flow behavior. All the other figures Figure-8 (b), 8 (c) and 8 (d) shows the comparison of different models for predicting pressure coefficient. In Figure-8 (b) and 8 (c), Transition SST model and SST k-ω model produce very similar results whereas RNG k-ε model also produce similar results for the lower side and shows a little deviation in the upper side of the airfoil. Laminar and Transition k-kl-ω generate results with a higher deviation with other models. In Figure-8 (c) all the models shows similar characteristics. On the otherhand in Figure-8 (d), no model generate similar result for the upper side but for the lower side, all the models generate similar results with small deviations.

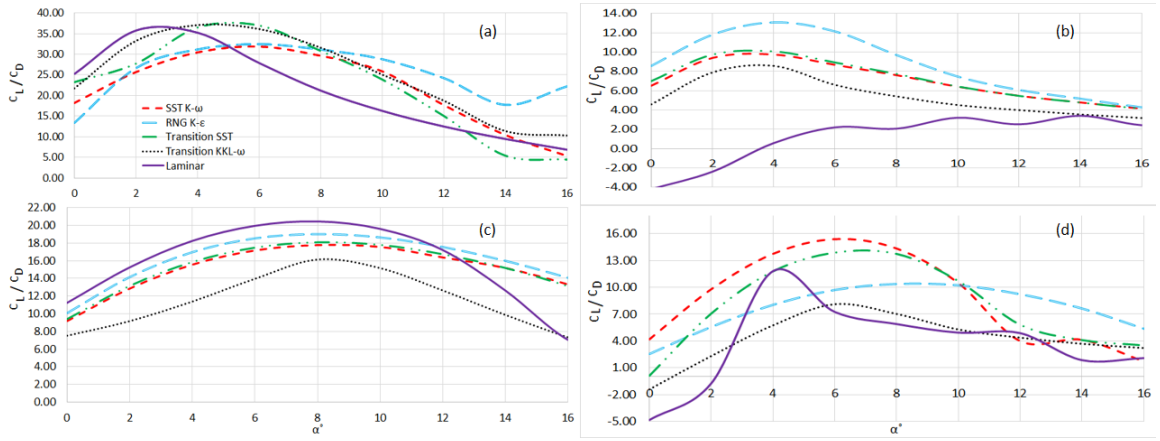

Figure-9. A comparison of numerical data between the viscous models for lift-to-drag ratio (C_L/C_D) vs angle of attack (α) for the airfoils: (a) NACA 4412, (b) NACA 4418, (c) NACA 4421 and (d) NACA 2412.

Figure-9 illustrates the lift-to-rag ratio (C_L/C_D) of the above airfoils for different viscous models. In general, turbulent models show similar results, whereas laminar model demonstrate large deviation in majority cases. Regardless of airfoil profiles, a peak C_L/C_D exist, which appears to be model dependent. The location of this peak is also not confined within a narrow band of α. The C_L/C_D is found to be the highest peak within 3˚-6˚ for NACA 4412 (Figure-9 (a)), 3˚-5˚ for NACA 4418 (Figure-9 (b)), around at α=8˚ for NACA 4421. Besides, NACA 2412 shows different locations of the highest C_L/C_D for different models (Figure-9 (d)). Only RNG k-ε model predict highest C_L/C_D at α=8˚ and within 4˚-6˚ for other models.

Figure-10 depicts the streamlines of the flow for a low Reynolds number (Re ≈ 20,000 at 3 m/s wind speed) at three different angles of attack (α=10˚, α=14˚ and α=16˚). The angle of attacks are chosen such that the flow behavior represent before stall, at or around stall and after stall. It appears that for NACA 4412 (Figure-10 (a)), with increase of α the wake region behind the airfoil slowly increases. The flow separation point approaches closer to the upstream points as α increases. For NACA 4418 (Figure-10 (b)), the flow is smooth and qualitatively similar to NACA 4412 for α=10˚ and α=14˚. However, at α=16˚ a distinctly different flow pattern is predicted and turbulence dominates the flow in the downstream region due to flow separation. A similar flow behaviors for NACA 4421 and NACA 2412 is predicted in Figure-10 (c) and Figure-10 (d), respectively.

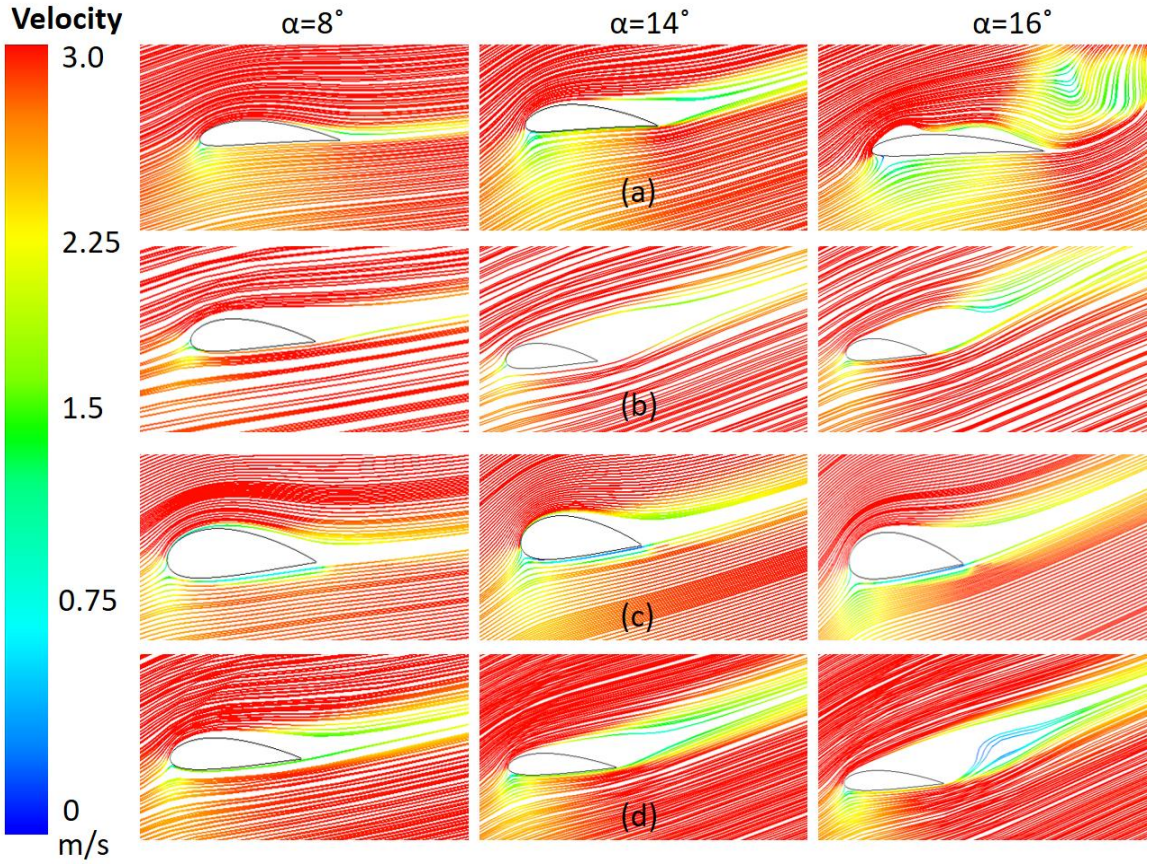

Figure-10. A comparison between the airfoils according to the streamlines at Re ≈ 20,000 for (a) NACA 4412, (b) NACA 4418, (c) NACA 4421, and (d) NACA 2412 at α=8˚, α=14˚, and α=16˚ respectively

4. CONCLUSIONS

Viscous model has significant impact on the numerical result of flow simulations for low Reynolds number study. A comparative analysis between different viscous models have been presented in this study. Four different airfoils have been investigated by five different viscous models. The numerical data have been compared with the experimental results from reliable sources to validate the numerical analysis. For low Reynolds number study, laminar model perform very well for low angle of attack (α) until the stall angle. After the stall angle laminar model can no longer predict the lift coefficient accurately where RNG k-ε model and SST k-ω model perform better. All these models perform very well to predict coefficient of pressure for the lower side of the airfoil but due to flow separation, no model generate accurate results for the upper side. The study shows that, laminar model, RNG k-ε model and SST k-ω model can be very useful whereas Transitional k-kl-ω model will generate anomalous results and the Transitional SST model performs moderately and for some cases generate inaccurate results. The present work can be useful for further low Reynolds number studies.

ACKNOWLEDGEMENTS

Bangladesh Bureau of Educational Information & Statistics, Ministry of Education, Government of the People's Republic of Bangladesh is acknowledged for the grants provided for this work via GARE (PS2017520).

REFERENCES

[1] N. K. Siavash, G. Najafi, T. T. Hashjin, B. Ghobadian, E. Mahmoodi. 2020. Mathematical modeling of a horizontal axis shrouded wind turbine. Renewable Energy. 146: 856-866.

[2] R. Mereu, S. Passoni, F. Inzoli. 2019. Scale-resolving CFD modeling of a thick wind turbine airfoil with application of vortex generators: Validation and sensitivity analyses, Energy. Vol. 187.

[3] I. C. M. Lositano, L. A. M. Danao. 2019. Steady wind performance of a 5 kW three-bladed H-rotor Darrieus vertical axis wind turbine (VAWT) with cambered tubercle leading edge (TLE) blades, Energy. 175: 278-291.

[4] A. Meana-Fernández, J. M. F. Oro, K. M. A. Díaz, M. G. Vega, S. Velarde-Suárez. 2019. Application of Richardson extrapolation method to the CFD simulation of vertical-axis wind turbines and analysis of the flow field. Engineering Applications of Computational Fluid Mechanics. 13(1): 359-376.

[5] X. Cai, Y. Zhang, W. Ding, S. Bian, The aerodynamic performance of H-type darrieus VAWT rotor with and without winglets: CFD simulations, Energy Sources, Part A: Recovery, Utilization, and Environmental Effects, Taylor & Francis Online, 2019. DOI: 10.1080/15567036.2019.1691286.

[6] M. M. Elsakka, D. B. Inghama, L. Maa, M. Pourkashaniana. 2019. CFD analysis of the angle of attack for a vertical axis wind turbine blade. Energy Conversion and Management. 182: 14-165.

[7] T.-T. Zhang, M. Elsakka, W. Huang, Z. Wang, D. B. Ingham, L. Ma, M. Pourkashanian. 2019. Winglet design for vertical axis wind turbines based on a design of experiment and CFD approach. Energy Conversion and Management. 195: 712-26.

[8] Y. Wang, H. Tong, H. Sima, J. Wang, J. Sun, D. Huang. 2019. Experimental study on aerodynamic performance of deformable blade for vertical axis wind turbine. Energy. 181: 18-201.

[9] S. G. Horcas, M. H. A. Madsen, N. N. Sorensen, F. Zahle. 2019. Suppressing vortex induced vibrations of wind turbine blades with flaps. Recent Advances in CFD for Wind and Tidal Offshore Turbines. pp. 11-24.

[10] M. Mashud, Shabnoor M. Joty and Zahir U. Ahmed. 2021. Optimization of Low Speed Wind Turbine Blade Profile on the Basis of Lift Coefficient, ARPN Journal of Engineering and Applied Sciences (ISSN 1819-6608) Vol:16 No:02, pp. 112-120.

[11] S. M. Shinde, M. Chaudhari, T. Jeurkar, S. Kadam, K. B. Salunkhe. 2018. Design and analysis of coaxial rotor wind turbine, Proceedings of International Conference on Intelligent Manufacturing and Automation. pp. 69-80.

[12] M. Kaya. 2019. A CFD based application of support vector regression to determine the optimum smooth twist for wind turbine blades, Sustainability. 11(16).

[13] Z. Ni, M. Dhanak, T. Su. 2019. Improved performance of a slotted blade using a novel slot design. Journal of Wind Engineering & Industrial Aerodynamics. 189: 34-44, 2019.

[14] E. Arteaga-Lopez, C. Angeles-Camacho, F. Banuelos-Ruedas. 2019. Advanced methodology for feasibility studies on building-mounted wind turbines installation in urban environment: Applying CFD analysis, Energy. 167: 181-188.

[15] R. V. Rodrigues, C. Lengsfeld. 2019. Development of a computational system to improve wind farm layout, Part II: Wind Turbine Wakes Interaction, Energies. 12(7).

[16] M. Costantini, C. Fuchs, U. Henne, C. Klein, V. Ondrus, M. Bruse, M. Löhr, M. Jacobs. 2019. A reliable experimental methodology for the study of wind-turbine rotor blade aerodynamics, Journal of Physics: Conf. Series, vol. 1222, Wind Europe Conference and Exhibition, Bilbao, Spain.

[17] G. Li, X. Huang, Y. Jiang, C. Qin. 2019. An experimental study of the dynamic aerodynamic characteristics of a yaw-oscillating wind turbine airfoil, Phys. Fluids. 31: 067102.

[18] Q. Li, J. Xu, Y. Kamada, T. Maeda, S. Nishimura, G. Wu, C. Cai. 2019. Experimental investigations of airfoil surface flow of a horizontal axis wind turbine with LDV measurements, Energy. 191: 116558.

[19] S. Deshmukh, S. Bhattacharya, A. Jain, A. Ranjan Paul. 2019. Wind turbine noise and its mitigation techniques: A review. 2nd International Conference on Energy and Power, ICEP2018, 13-15 December 2018, Sydney, Australia. Energy Procedia. 160: 633-640.

[20] C. E. Lin, B. C. Phan, J.-S. Chuang. 2019. Small wind generation using complex airfoil turbine, Cogent Engineering. 6: 1687073.

[21] M. Lipian, M. Kulak, M. Stepien. 2019. Fast Track Integration of Computational Methods with Experiments in Small Wind Turbine Development. Energies. 12, 1625; doi:10.3390/en12091625

[22] P. Giguere, M. S. Selig. 1998. New Airfoils for Small Horizontal Axis Wind Turbines. Journal of Solar Energy Engineering. Vol. 120 I 109.

[23] R. K. Singh, M. R. Ahmed, M. A. Zullah, Y. H. Lee. 2012. Design of a low Reynolds number airfoil for small horizontal axis wind turbines. Renewable Energy. 42: 66e76.

[24] X. Li, L. Zhang, J. Song, F. Bian, K. Yang. 2020. Airfoil design for large horizontal axis wind turbines in low wind speed regions, Renewable Energy. 145: 2345-2357.

[25] A. K. Wright, D. H. Wood. 2004. The starting and low wind speed behaviour of a small horizontal axis wind turbine. Journal of Wind Engineering and Industrial Aerodynamics. 92: 1265-1279.

[26] P. R. Ebert, D. H. Wood. 1997. Observations of the Starting Behaviour of a Small Horizontalaxis Wind Turbine. Renewable Energy. 12(3): 245-257.

[27] M. A. Sayed, H. A. Kandil, A. Shaltot. 2012. Aerodynamic analysis of different wind-turbine-blade profiles using finite-volume method. Energy Conversion and Management. 64: 541-550.

[28] X. Shen, E. Avital, G. Paul, M. A. R., P. Wen, T. Korakianitis. 2016. Experimental study of surface curvature effects on aerodynamic performance of a low Reynolds number airfoil for use in small wind turbines. JOURNAL OF RENEWABLE AND SUSTAINABLE ENERGY. 8, 053303. doi: 10.1063/1.4963236

[29] H. Xi, W. J. Jun, Y. M. Qing, M. A. D. Li, Y. Chao, L. P. Qing. 2017. Numerical simulation of gurney flaps lift-enhancement on a low Reynolds number airfoil, Sci China Tech Sci. 60: 1-12, doi: 10.1007/s11431-017-9085-4

[30] H. Dong, T. Xia, L. Chen, S. Liu, Y. D. Cui, B. C. Khoo, A. Zhao. 2019. Study on flow separation and transition of the airfoil in low Reynolds number, Phys. Fluids. 31, 103601.

[31] J. Deng, L. Sun, X. Shao. 2019. Wake dynamics of low-Reynolds-number flow around a two-dimensional airfoil. Phys. Fluids. 31, 024102.

[32] G. D. Ilio, D. Chiappini, S. Ubertini, G. Bella, S. Succi. 2018. Fluid flow around NACA 0012 airfoil at low-Reynolds numbers with hybrid lattice Boltzmann method, Computers and Fluids.

[33] M. Drela, XFOIL: 1989. An Analysis and Design System for Low Reynolds Number Airfoils. In: Mueller T.J. (eds.) Low Reynolds Number Aerodynamics. Lecture Notes in Engineering, vol. 54. Springer, Berlin, Heidelberg.

[34] J. Morgado, R. Vizinho, M. A. R. Silvestre, J. C. Páscoa. 2016. XFOIL vs CFD performance predictions for high lift low Reynolds number airfoils, Aerospace Science and Technology.

[35] J. C. Chua, N. S. Lopez, G. Augusto. 2017. Numerical and statistical analyses of aerodynamic characteristics of low Reynolds number airfoils using Xfoil and JMP. AIP Conference Proceedings 1905, 050016.

[36] W. A. Timmer, R. P. J. O. M. van Rooij. 2003. Summary of the Delft University Wind Turbine Dedicated Airfoils. Journal of Solar Energy Engineering · January. DOI: 10.1115/1.1626129.

[37] S. Zhang, H. Li, A. A. Abbasi. 2019. Design methodology using characteristic parameters control for low Reynolds number airfoils, Aerospace Science and Technology.

[38] J. Wauters, J. Degroote. 2018. On the study of transitional low-Reynolds number flows over airfoils operating at high angles of attack and their prediction using transitional turbulence models, Progress in Aerospace Sciences, 103: 52-68. DOI: 10.1016/j.paerosci.2018.10.004

[39] D. Lee, T. Nonomura, A. Oyama, K. Fujii. 2017. Comparative studies of numerical methods for evaluating aerodynamic characteristics of two-dimensional airfoil at low Reynolds numbers. International Journal of Computational Fluid Dynamics, vol. 31. DOI: 10.1080/10618562.2016.1274398.

[40] S. M. A. Aftab, A. S. M. Rafie, N. A. Razak, K. A. Ahmad. 2016. Turbulence model selection for low Reynolds number flows. PLoS ONE 11(4): e0153755. doi:10.1371/journal.pone.0153755

[41] G. Santo, M. Peeters, W. V. Paepegem, J. Degroote. 2019. Analysis of the aerodynamic loads on a wind turbine in off-design conditions, In: Ferrer E., Montlaur A. (eds) Recent Advances in CFD for Wind and Tidal Offshore Turbines. Springer Tracts in Mechanical Engineering. Springer, Cham. pp. 51-59.

[42] S. H. Kim, K. Suh. 2019. Experimental and numerical investigation on power characteristics of 300 W class horizontal axis wind turbine with wave winding type AFPM Generator. International Journal of Precision Engineering and Manufacturing-Green Technology, 2019. DOI: 10.1007/s40684-019-00160-y.

[43] M. H. Mohamed, A. Dessoky, F. Alqurashi. 2019. Blade shape effect on the behavior of the H-rotor

Darrieus wind turbine: Performance investigation and force analysis, Energy. 179: 1217-1234.

[44] R. K. Singh, M. R. Ahmed. 2013. Blade design and performance testing of a small wind turbine rotor for low wind speed applications. Renewable Energy. 50: 812e819.

[45] N. Thomareis, G. Papadakis. 2017. Effect of trailing edge shape on the separated flow characteristics around an airfoil at low Reynolds number: A numerical study, PHYSICS OF FLUIDS 29, 014101.

[46] Ansys® Academic Research Fluent, Release 12.0, Help System, Ansys Fluent 12.0 Theory Guide, Chapter 4: Turbulence, ANSYS, Inc, 2009.

[47] I. H. Abbott, A. E. V. Doenhoff, L. S. Stivers Jr. 1945. Summary of airfoil data (Report No. 824), US National Advisory Committee for Aeronautics.

[48] D. Heffley. Aerodynamic characteristics of a NACA 4412 airfoil, Retrieved from https://www.baylor.edu/content/services/document.php/41147.pdf

[49] D. Coles, A. J. Wadcock. 1979. Flying-hot-wire study of flow past an NACA 4412 airfoil at maximum lift, American Institute of Aeronautics and Astronautics (AIAA) Journal. 17: 321-329.